SCIENTIFIC REP♦RTS

OPEN

Efficient 3D-Silver Flower-like Microstructures for Non-Enzymatic Hydrogen Peroxide (H$_2$O$_2$) Amperometric Detection

Gumaa A. El-Nagar[1,2], Radwan M. Sarhan[1,3,4], Ahed Abouserie[5], Natalia Maticiuc[6], Matias Bargheer[3], Iver Lauermann[6] & Christina Roth[2]

We present an efficient non-enzymatic hydrogen peroxide sensor composed of flower-like silver microstructures. The silver microstructures´ morphology is controlled by adding minute amounts of either succinic or malonic acid as directing agents. Morphologically, silver particles showed ball-like structures in the absence of both directing agents, while the presence of 50 ppm of succinic acid and malonic acid lead to monodisperse chrysanthemum and water-lily flower-like structure, respectively. A higher concentration of succinic acid resulted in a rose flower-like structures. Electrochemically, the rose flower-like silver microstructures exhibited the best performance for H$_2$O$_2$ detection as evaluated by their outstanding electrocatalytic activity (12 times higher) and sensitivity (2.4 mM^{-1} cm^{-2}, 24 times higher) with lower detection limit (0.4 µM, 5 times smaller) together with their excellent H$_2$O$_2$ selectivity compared to that of the ball-shaped structures. Additionally, rose-flower microstructures exhibited excellent long-term stability; 11 and 3 times higher compared to ball- and water-lily structures, respectively. This substantial performance enhancement is attributed to their unique flower-like structure providing a higher number of active surface sites (at least 8 times higher) and a faster detachment rate of *in-situ* generated oxygen bubbles from their surface.

Hydrogen peroxide (H$_2$O$_2$) detection has recently attracted significant attention, thanks to its crucial role in a wide range of applications including biological systems, environmental protection together with food, pharmaceutical and clinical industries[1,2]. Thus, the development of an efficient (i.e., accurate, sensitive, selective and rapid) low-cost H$_2$O$_2$ sensor is extremely important. Several H$_2$O$_2$ detection methods have been employed such as spectrophotometry[3], chromatography[4], chemiluminescence[5,6], titrimetry[7] and electrochemistry[8–11]. Electrochemical methods using enzyme-based biosensors are the most appropriate and effective tool for H$_2$O$_2$ detection owing to their unique features including low cost, high selectivity, simplicity, and excellent sensitivity. However, the low stability, limited lifetime and the complicated immobilization procedures of the enzyme-based catalysts together with their susceptibility to change with the operating environment (e.g., pH, temperature, toxic chemicals) limit their practical applications[12–14].

As a result, the development of stable and efficient H$_2$O$_2$ non-enzymatic sensors is urgently required. In this regard, various metal nanoparticles (e.g., AuNPs, PtNPs, PdNPs, AgNPs)[15–19] and metal oxide nanostructures (e.g., MnO$_2$, Fe$_2$O$_3$, etc)[20–22] are alternatively employed. Among them, silver nanoparticles (AgNPs) have aroused increasing interest due to their unique combination of biocompatibility and highest electrical conductivity together with their outstanding electrocatalytic activity[23,24]. But their structure agglomeration, collapse and segregation during long-term measurement results in diminished performance. Thus, the development of a catalyst with a high mechanical stability and robust structure is required for efficient H$_2$O$_2$ detection.

[1]Department of Chemistry, Faculty of Science, Cairo University, Giza, 12613, Egypt. [2]Institut für Chemie und Biochemie Physikalische und Theoretische Chemie, Freie Universität Berlin, 14195, Berlin, Germany. [3]Institute of Physics and Astronomy, University of Potsdam, Karl-Liebknecht-Strasse 24–25, 14476, Potsdam, Germany. [4]Humboldt-Universität zu Berlin, School of Analytical Sciences Adlershof (SALSA), Albert-Einstein-Str. 5–9, 10099, Berlin, Germany. [5]Institute of chemistry, University of Potsdam, Karl-Liebknecht-Strasse 24–25, Potsdam, D-14476, Germany. [6]Helmholtz-Zentrum Berlin für Materialien und Energie, Hahn-Meitner-Platz 1, 14109, Berlin, Germany. Correspondence and requests for materials should be addressed to G.A.E.-N. (email: Gumaa.elnagar@fu-berlin.de)

1

In this paper, an efficient and stable non-enzymatic H_2O_2 sensor of 3D-silver microflowers with different roughness and shapes is introduced. Dicarboxylic acids (i.e., malonic and succinic acids) were used as capping agents in order to (a) stabilize the growth of silver nanoparticles, as well as protect them from agglomeration and losing their surface features and (b) controlling their morphology and roughness via the interaction (e.g., electronic interaction, strong hydrogen-bonding, or weak van der Waals interactions) between the malonic and succinic acids functionalities (carboxylic groups) with the silver nanoparticles. Different concentrations of succinic and malonic acids were used to prepare silver microparticles with various geometries (i.e., ball and flower-like structures). The effect of the *in-situ* formed oxygen bubbles size atop of the as-prepared electrodes and their accumulation/detachment rate on the stability of the suggested electrodes are investigated, for the first time. All prepared silver microstructures are dispersed in a stable chitosan matrix to avoid their aggregation/sintering.

Experimental

Chemicals.   Silver nitrate, succinic acid, malonic acid, uric acid, urea, glucose, potassium hydroxide, chitosan and ascorbic acid were all purchased from Sigma-Aldrich and were used as received without any further purification. All solutions were prepared using deionized water with resistivity of 18.2 MΩ cm which was prepared using a Milli-Q reagent deionizer (Millipore).

Silver Microstructures Synthesis and Fabrication.   Hierarchical silver microflowers were synthesized via a previously described procedure with a little modification[25]. Ascorbic acid was used as a reducing agent while different dicarboxylic acids were used as structure-directing agents as well as capping agents. This results in formation of silver structures with various morphologies ranging from silver microspheres to 3D silver microflowers. Briefly, 1 ml of 1 M of aqueous solution of $AgNO_3$ and 50 μL of 0.25 M aqueous solution of succinic acid were mixed in 10 ml of deionized water for 10 min in an ice-water bath. To initiate the formation of microstructures, 1 ml of 1 M aqueous solution of ascorbic acid was then quickly added and vigorously stirred for 15 min. The solution color turned from colorless to dark grey immediately and finally a large quantity of the silver particles precipitated. The silver microstructures were then collected and washed several times with deionized water and dried under vacuum. This resulted in the formation of silver microstructures with chrysanthemum flower-like structures. Doubling the concentration of succinic acid resulted in rose flower-like structures. The same procedures were used to synthesize water-lily flower like structures, by replacing the succinic acid with malonic acid as a directing agent. For sake of comparison, the silver microparticles were prepared without adding a structure-directing agent. This resulted in the formation of the ball-shaped silver microstructures.

Electrode preparation was performed as follows.   5 mg of the above obtained silver microstructure powders were dispersed into 3 ml of chitosan solution (0.5%) and sonicated for 15 minutes. Then, 10 μl of the obtained suspension was drop-cast atop of a previously mechanically cleaned glassy carbon electrode (GCE) using alumina powder and allowed to dry at room temperature. To prepare a solution of the poorly soluble chitosan, 0.5 g of chitosan was dissolved in 1% acetic acid aqueous solution overnight. The chitosan matrix is used to stabilize the silver structures so that they will resist to structure deformation and aggregation during long-term measurements.

Electrodes Characterization.   All the electrochemical tests were performed at room temperature in a conventional three-electrode glass cell using a Gamry setup potentiostat/Galvanostat, where a coiled Pt wire and a saturated calomel electrode (SCE) served as a counter and reference electrode, respectively. Electrochemical impedance spectroscopy (EIS) measurements were carried out at −0.25 V (N.B., Nyquist plot was first measured at different potentials and −0.25 V was selected as the best potential, at which the kinetic control region can be easily observed) with a disturbance potential of 5 mV and a frequency range from 1 MHz to 0.1 Hz. A scanning electron microscope coupled with an energy dispersive X-ray spectrometer (JEOL JSM-6510) was used to evaluate the electrode morphology and composition. X-ray diffraction (XRD using STOE STADI) in transmission geometry XRD was performed with Cu K$_\alpha$ radiation ($\lambda = 1.54$ Å) and position sensitive detector to identify the crystallographic structure of the as prepared silver microstructures. X-ray photoelectron spectroscopy (XPS, CLAM4 electron analyzer from Thermo VG scientific), using a Mg Kα X-ray source (1254 eV) was used to determine the samples chemical composition. For evaluation, a linear background was subtracted and peaks were fitted using Voigt functions with identical FWHM for each component of the same element.

Results and Discussion

Material and Electrochemical Characterizations.   The morphology and structure of the as-prepared silver catalysts were examined by SEM and XRD, as seen in Fig. 1. Silver microparticles with ball-like structures were obtained in the absence of both directing agents (i.e., malonic and succinic acids) with an average ball-diameter of 2 μm (see Fig. 1A, assigned as Ag$_{ball}$/GCE, color code black). Interestingly, the presence of a minute amount of malonic acid (~50 ppm) resulted in the formation of monodisperse and homogenous water-lily flower-like silver structures composed of well-assembled and loosely packed silver nanosheets (Fig. 1B, denoted as Ag$_{lily-flower}$/GCE, color code red). Using higher malonic acid concentration (~100 ppm) yielded water-lily flower - like structures as well (see Fig. 1C), but with more loosely packed silver nanosheets compared to that prepared with 50 ppm solution. We only discuss the electrocatalytic behavior of the water-lily flowers prepared by 50 ppm, since they yield a better electrocatalytic performance attributed to their higher electroactive surface area originating from their higher amount of loosely packed silver nanosheets, as well as their smaller average sheets size (ca. 42 nm as estimated from its XRD using Scherrer's equation[14]) compared to that of lily-flower structures (with estimated average particle size of ca. 69 nm) obtained using higher malonic acid concentration. Attempts to use even lower concentrations down to 10 ppm, malonic acid resulted in disordered silver sheet-like structures (data not shown). It is clear that the acid induces formation of the nanosheets. The use of succinic acid (~50 ppm) as
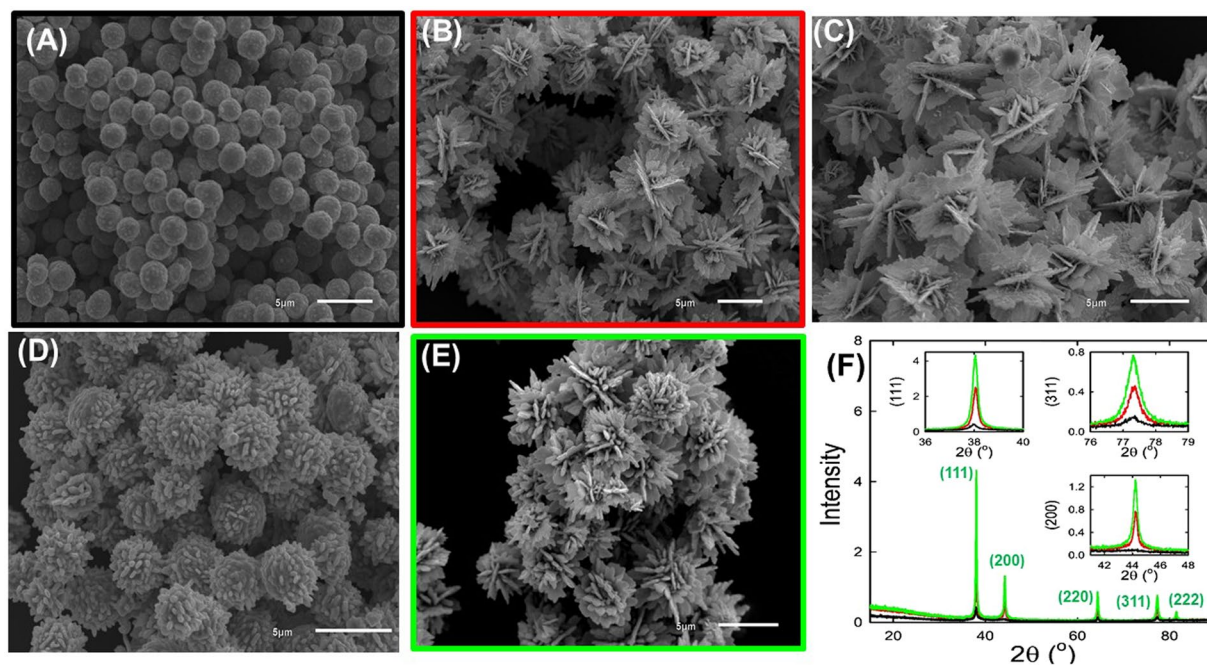
Figure 1. (**A–E**) SEM images of silver microstructures prepared (**A**) in the absence of directing agents and in the presence of (**B**) 50 ppm malonic acid, (**C**) 100 ppm malonic acid, (**D**) 50 ppm succinic acid and (**E**) 100 ppm succinic acid. Frames color code the graphs in panel (**F**): XRD pattern of ball (Ag$_{ball}$, black-line), lily-flower (Ag$_{lily-flower}$, red-line) and rose-flower (Ag$_{Rose-flower}$, green-line) with assigned Miller indices. Insets show zooms into the (111), (200) and (311) reflections.

a directing agent resulted in the creation of chrysanthemum flower-like structures, which is mainly ball-shaped structures with short protrusions (see Fig. 1D, referred as Ag$_{chrysanthemums-flower}$/GCE).

Interestingly, using higher succinic concentration (~100 ppm, notated as Ag$_{Rose-flower}$/GCE, color code green) showed rose-flower silver like structures (see Fig. 1E) with much better electrocatalytic performance for hydrogen peroxide electrosensing. These results indicate the essential role of the directing agents (i.e., malonic and succinic acid) in controlling the silver particles morphology and roughness. However, the assembly of these nanostructures is significantly influenced by the added amount of the dicarboxylic acids as directing agents, the mechanism of such assembly is still unclear. For examples, very low concentration of succinic and malonic acids down to 10 ppm led to formation of non-assembled silver nanosheets structures, therefore, we suggest that the added acids might form complexes with the silver ions or adsorb on the surface of the silver nucleates and induce a new way of assembly leading to different morphology.

The crystallographic orientation and the crystallinity of the as-prepared silver catalysts were further investigated by XRD. As revealed in Fig. 1F, all the three tested silver catalysts (in absence and in the presence of malonic or succinic acids) exhibited the typical five diffraction peaks of the face-centered cubic (fcc) Ag crystal phase, these diffraction peaks can be indexed to the (111), (200, (220), (311), and (222) crystal planes of the as-prepared silver structures. Furthermore, using both directing agents led to smaller crystallite sizes as evidenced by their broader reflection peaks, besides, the directing agents existence resulted in smaller negative shift in all reflection peaks. This might be suggested electronic interaction between directing agents and silver nanoparticles which is confirmed next using XPS technique. *XPS spectra of the silver nanoparticles obtained in the absence of both directing agents (Ag$_{ball}$) and in the presence of 100 ppm of succinic acid and 100 ppm malonic acid were further investigated to determine if their presence might exert any electronic effect on the silver nanoparticles. As revealed in* Fig. 2A, *the presence of 100 ppm of succinic acid (curve c, green-color) or 100 ppm malonic acid (curve b, red-color) resulted in approx. 0.1 eV and 0.07 eV negative shift of the Ag3d doublet peaks compared to that of Ag$_{ball}$ (curve a, black-line), respectively. This might be suggested strong electronic interaction between silver nanoparticles and the directing agents.*

Figure 2B shows the characteristic voltammetric (CVs) behavior of the three studied catalysts in 0.5 M potassium hydroxide (KOH). As seen in this figure, all of them exhibited the typical characteristic behavior of a clean polycrystalline silver electrode, where two main redox peak couples I/I´ and II/II´ are observed in their respective cyclic voltammograms (CVs) attributed to the successive oxidation at the surface of the Ag particles from Ag to Ag^{2+} [15]. Interestingly, the Ag$_{lily-flower}$/GCE (using 50 ppm malonic acid, red-line, curve b) and Ag$_{Rose-flower}$/GCE (using 100 ppm succinic acid, green-line, curve c) exhibited higher peak intensities (i.e., II/II´) compared to that of the Ag$_{ball}$/GCE (black-line, curve a). This indicates that Ag$_{lily-flower}$/GCE and Ag$_{Rose-flower}$/GCE electrodes have a higher surface area compared to that of the Ag$_{ball}$/GCE electrode.

The electrochemically active surface area of the as-prepared Ag microstructures was estimated by lead under potential deposition (UPD) stripping [15] using the standard reported value of 400 µC/cm^2 (see inset of Fig. 2B). The estimated active surface area was 0.9, 3.3 and 8 cm^2 for the Ag$_{ball}$/GCE, Ag$_{lily-flower}$/GCE and Ag$_{Rose-flower}$/GCE
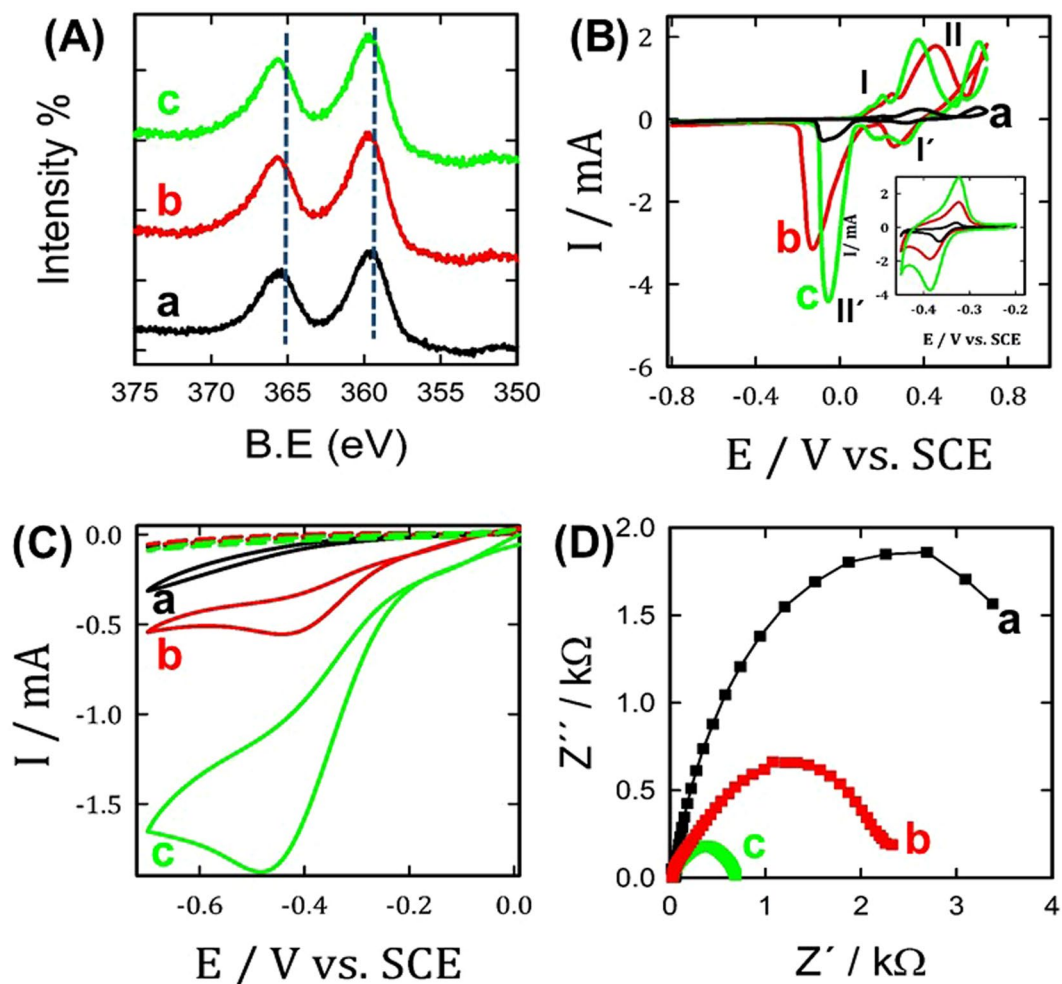
Figure 2. (**A**) High resolution Ag 3d XPS spectra of different studied silver microstructures; Ag$_{ball}$ (black-line, curve a), Ag$_{lily-flower}$ (red-line, curve b) and Ag$_{Rose-flower}$ (green-line, curves c), (**B**) CVs obtained at same silver microstructures (same color code from Fig. 2A); Ag$_{ball}$ (curve a), Ag$_{lily-flower}$ (curve b) and Ag$_{Rose-flower}$ (curve c) in 0.1 M KOH with a scan rate of 0.1 V/s (inset shows the Pb (UPD) stripping measured in 0.1 M HCl containing 10 mM Pb(NO$_3$)$_2$), (**C**) CVs measured at the same electrodes in the absence (dashed-lines) and in the presence of 1 mM H$_2$O$_2$ (solid-lines) in 0.1 M KOH with a potential scan rate of 0.02 V/s (same color code as in Fig. 2A. For E/V vs. SCE > 0, the graph mimic the response seen in panel A) and (**D**) Nyquist plots obtained at the same electrodes in 0.1 M KOH containing 1 mM H$_2$O$_2$ at −0.25 V vs. SCE (same color code as in Fig. 2A).

electrodes, respectively. That is, Ag$_{Rose-flower}$/GCE exhibited 8 and 2.4 times higher active surface area compared to Ag$_{ball}$/GC and Ag$_{lily-flower}$/GC electrodes, respectively.

The electrocatalytic activity of the as-prepared catalysts towards hydrogen peroxide electrosensing was further investigated by CVs. Figure 2C shows the CVs of the Ag$_{ball}$/GCE, Ag$_{Rose-flower}$/GCE and Ag$_{lily-flower}$/GCE electrodes in 0.1 KOH aqueous solution in the absence (dashed-lines) and presence of 10 mM H$_2$O$_2$ (solid-lines). As shown in this figure, in the absence of H$_2$O$_2$ (dashed-lines) only a small current was observed. The addition of 10 mM H$_2$O$_2$ resulted in a significant increase of the reduction current (solid-lines) attributed to the reduction of H$_2$O$_2$ according to the following equation:

$$H_2O_2 \Rightarrow H_2O + \frac{1}{2}O_2$$
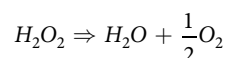
Interestingly, Ag$_{lily-flower}$/GCE (red-line) and Ag$_{Rose-flower}$/GCE (green-line) electrodes exhibited outstanding activity compared to that of the Ag$_{ball}$/GCE (black-line) electrode as evaluated by the significant positive shift of the onset potential together with the much higher current intensity of H$_2$O$_2$ reduction. That is, the Ag$_{Rose-flower}$/GCE electrode showed 12 and 4 times higher electrocatalytic activity relative to that of Ag$_{ball}$/GC and Ag$_{lily-flower}$/GCE electrodes, respectively. This significant activity improvement of Ag$_{Rose-flower}$/GCE electrode for H$_2$O$_2$ reduction is attributed to their higher surface area and unique flower-like structures.

It is worth to mention here that Ag$_{Rose-flower}$/GCE (using 100 ppm succinic acid) exhibited higher activity and performance compared to Ag$_{chrysanthemums-flower}$/GCE (using 50 ppm succinic acid), data not shown. Additionally, Nyquist plots (Fig. 2D) were measured at the as-prepared silver nanostructures which are obtained in the absence

Sensors	Sensitivity (mA mM^{-1}cm^{-2})	Detection limit (μM)	Linear range (mM)	References
Ag NW NT assembly	1.340	0.6	Up to 3.4	26
Ag NW colloid	0.00515	1.5	Up to 21.3	27
Ag NW colloid + graphene	0.01237	1.0	Up to 34.3	27
Electrodeposited Ag NW	0.374	334	Up to 10.1	28
Ag dendrites	0.0518	0.7	Up to 1.5	29
Ag-MnO$_2$-MWCNTs/GCE	0.0825	1.7	Up to 10.4	30
Pt@Au NPS	0.3134	0.6	Up to 0.45	31
Pd core-Pt NDs-rGO	0.6728	0.03	Up to 0.1	32
Fe$_3$O$_4$/RGO	0.688	3.2	Up to 6.0	33
Ag$_{Rose-flower}$/GCE	2.4	0.4	Up to 14	This work
Agball/GCE	0.022	1.8	Up to 14	This work
Ag$_{lily-flower}$/GCE	0.480	1.0	Up to 14	This work

Table 1. A comparison of various non-enzymatic H$_2$O$_2$ sensors.
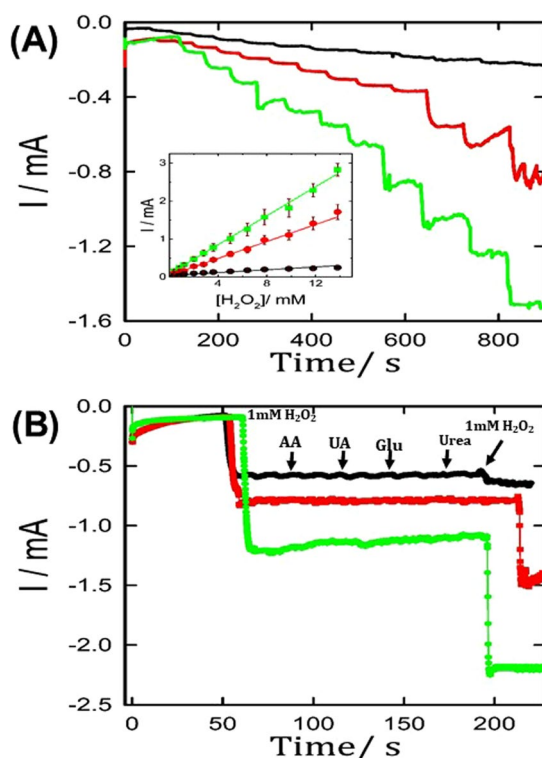
Figure 3. (**A**) Amperometric response (sensitivity test) obtained at silver microstructures in the absence (black-line) and presence of 50 ppm malonic (red-line) and 100 ppm succinic acid (green-line) with successive addition of H$_2$O$_2$ in N$_2$-saturated 0.1 M KOH performed at −0.4 V. The inset shows the stepwise increase in the concentrations, which leads to the stepwise response of the current (mA), same colors code as in Fig. 3A). (**B**) Amperometric response (selectivity test) of the same electrodes after adding 1 mM H$_2$O$_2$, 0.1 mM ascorbic acid (AA), glucose (Glu), uric acid (UA) and Urea, respectively (same colors code as in Fig. 3A).

of both directing agents (Ag$_{ball}$, black-line, curve a) and in the presence of 50 ppm malonic acid (Ag$_{lily-flower}$, red-line, curve b) or 100 ppm succinic acid (Ag$_{Rose-flower}$, green-line, curve c) to examine their charge transfer properties for hydrogen peroxide electroreduction. As shown in this figure, silver nanostructures (lily- and rose-flower structures) prepared using malonic and succinic acid as directing agents exhibited a lower charge transfer resistance compared to the silver nanoparticles obtained without using directing agents (ball-like structures).

The H$_2$O$_2$ electrosensing performance (e.g., selectivity, durability and sensitivity) of the suggested silver microstructure catalysts was then evaluated by amperometric technique. Figure 3A shows the sensitivity test of the three studied silver microstructures. As clearly seen in this figure, the Ag$_{Rose-flower}$/GCE electrode exhibited the best H$_2$O$_2$ electrosensing performance as demonstrated by its higher sensitivity with a rapid response time
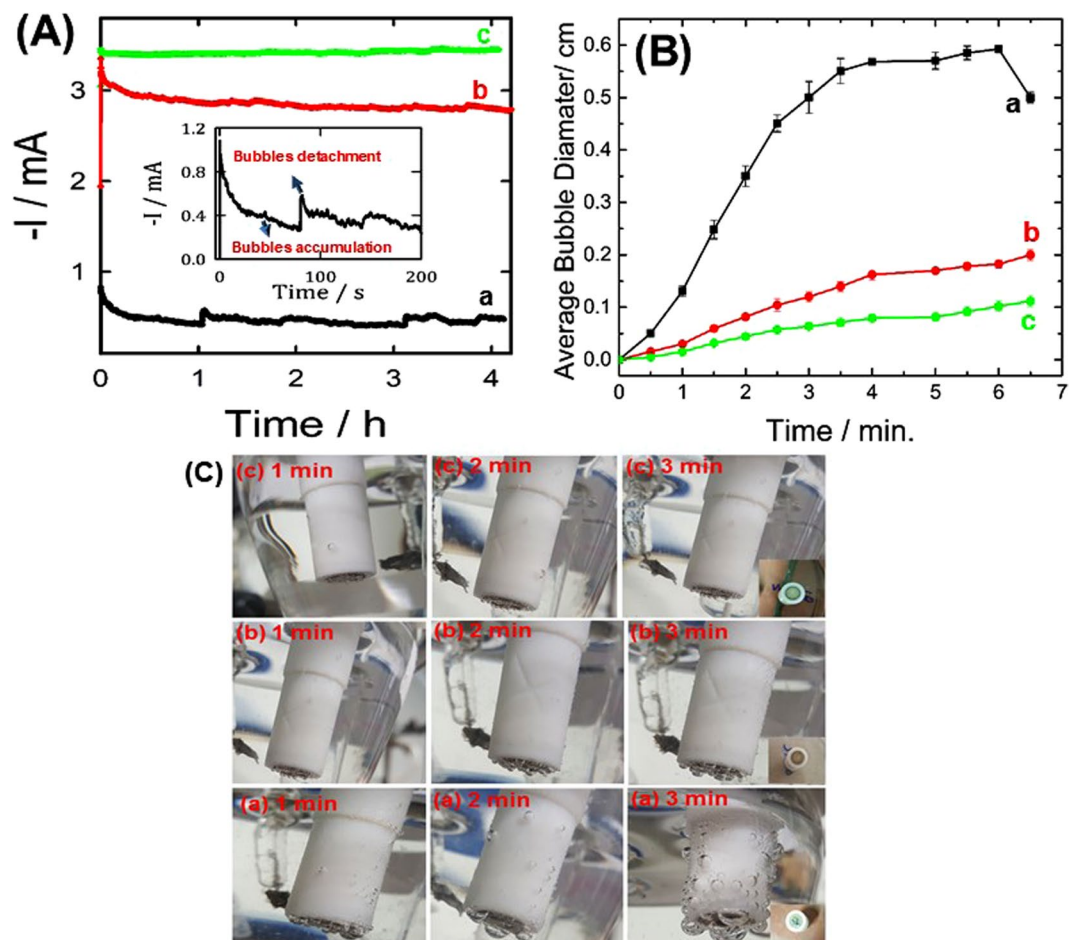
Figure 4. (**A**) current-transient (i–t) plots obtained at (a) Ag_{ball}/GCE, (b) $Ag_{lily-flower}$/GCE and (c) $Ag_{Rose-flower}$/GCE E in 0.1 M KOH containing 5 mM H_2O_2 at -0.3 V vs. SCE. (**B**) variation of average bubble diameter with time of (a) Ag_{ball}/GCE, (b) $Ag_{lily-flower}$/GCE and (c) $Ag_{Rose-flower}$/GCE and (**C**) the electronic images of the surface of the same electrodes at various times showing the bubble size and accumulation (same notations are used as in Fig. 4A, insets of these images show the surface of each electrode after measurement).

(2.4 mM mA^{-1} cm^{-2}, 24 times higher), lower detection limit (0.4 μM, 16 times lower) together with higher linear range (up to 14 mM) compared to the Ag_{ball}/GC electrode. Additionally, our proposed silver-based catalysts present a superior efficiency compared to various typical non-enzymatic H_2O_2 sensors (see Table 1). This enhanced H_2O_2 sensing efficiency at our proposed silver flower-like structures is attributed to their unique structures providing outstanding active surface areas with many hot-spot sites.

The interference-tolerance for the common interfering species (e.g., ascorbic acid, glucose, urea, uric acid) of the as-prepared silver-based catalysts was further investigated. As shown in Fig. 3B, all the studied silver microstructures-modified GCE electrodes exhibited an obvious amperometric response with the addition of 1 mM H_2O_2, while the successive addition of the above-mentioned interfering substances showed only a hardly discernible amperometric current response on the suggested sensors. This indicates the higher selectivity (i.e., high interference tolerance) of our proposed electrodes for non-enzymatic H_2O_2 sensing. Interestingly, both the $Ag_{lily-flower}$/GC and $Ag_{Rose-flower}$/GCE electrodes exhibited almost the same amperometric response of the first H_2O_2 addition after the second addition of H_2O_2 in the presence of the above-mentioned interfering species. On the other hand, the Ag_{ball}/GCE electrode only displayed 15% from its original amperometric response, indicating a higher stability and interference tolerance of flower-shaped silver microstructures compared to the Ag_{ball}/GCE electrode.

The current-transient curves (*i-t*) of all the studied silver-based sensors were performed in 0.1 M KOH containing 5 mM H_2O_2 at -0.3 V vs. SCE and the surface of these electrodes was imaged to estimate the effect of the *in-situ* formed oxygen bubbles size and their detachment rate on the as-prepared catalysts stability and performance, see Fig. 4. This figure shows the following interesting points:

(a) The catalytic stability of the Ag_{ball}/GCE electrode decays rapidly with time (see Fig. 4A-black-line, curve a) by about 45% after only 20 minutes of continuous H_2O_2 electrolysis. The catalytic activities of both $Ag_{lily-flower}$/GCE (red-line, curve b) and $Ag_{Rose-flower}$/GCE (green-line, curve c) electrodes were reduced by only 8% and 12%, indicating the higher stability of the silver flower-like microstructures.

(b) The oxygen bubbles generated by H_2O_2 reduction atop of the $Ag_{lily-flower}$/GCE are illustrated in panel b and $Ag_{Rose-flower}$/GCE (image c) electrodes are about 6 times smaller compared to that of the Ag_{ball}/GCE electrode (image a), see Fig. 4B. The rate of oxygen bubbles detachment from the $Ag_{lily-flower}$/GCE and $Ag_{Rose-flower}$/GCE surfaces is approximately 15 times faster compared that of the Ag_{ball}/GCE electrode. When the oxygen bubbles accumulate atop of the Ag_{ball}/GCE electrode and become larger, they block most of its surface-active sites. In other words, the rate of bubbles accumulation at the Ag_{ball}/GCE electrode is much faster than their detachment rate. This can explain the high stability and activity of the $Ag_{lily-flower}$/GC and $Ag_{Rose-flower}$/GCE electrodes compared to that of the Ag_{ball}/GCE electrode.

(c) As clearly seen in Fig. 4A, the stability of the Ag_{ball}/GCE electrode rapidly decreases due to the bubbles accumulation on its surface blocking their active-surface sites, then it restores partially its activity due to the bubbles detachment (see the inset of Fig. 4A). This process is repeated as clearly revealed from the observed spikes and the images of the electrode surface. There were no spikes observed for the $Ag_{lily-flower}$/GCE (Fig. 4A-curve c), indicating the higher bubbles detachment rate and their lower accumulation rate.

Conclusion

Silver microstructures with different morphologies (e.g., flower- and ball-like structures) have been successfully prepared via a facile one-step precipitation method. The as-prepared silver flower-like microstructures exhibited outstanding performance as non-enzymatic H_2O_2 sensors. They show 24 times higher sensitivity (2.4 mM^{-1} cm^{-2}) along with wider linear range (up to 14 mM) and smaller detection limit (about 0.4 µM, 16 times lower) compared to silver ball-like microstructures. This significant performance enhancement was attributed to their unique flower-like structures providing higher active surface area (8 times higher surface area) and facilitating the hydrogen peroxide reduction charge transfer together with the electronic interaction between the capping agents and silver nanoparticles. In addition, the suggested silver microflowers showed a much better stability about 11 and 3 times higher compared to that of silver nanoparticles with ball- and lily-flower like structures. Their higher stability was believed to originate from the smaller generated oxygen bubbles size and their faster detachment rates along with lower rate of bubbles accumulation on its surface relative to that of the silver ball-like structures.

References

1. Veal, E. A., Day, A. M. & Morgan, B. A. Hydrogen peroxide sensing and signaling. *Molecular cell* **26**, 1–14 (2007).
2. Laloi, C., Apel, K. & Danon, A. Reactive oxygen signalling: the latest news. *Current opinion in plant biology* **7**, 323–328 (2004).
3. Zhang, K. Stopped-flow spectrophotometric determination of hydrogen peroxide with hemoglobin as catalyst. *Talanta* **51**, 179–186 (2000).
4. Tarvin, M., McCord, B., Mount, K., Sherlach, K. & Miller, M. L. Optimization of two methods for the analysis of hydrogen peroxide: high performance liquid chromatography with fluorescence detection and high performance liquid chromatography with electrochemical detection in direct current mode. *Journal of chromatography. A* **1217**, 7564–7572 (2010).
5. Janasek, D. & Spohn, U. An enzyme-modified chemiluminescence detector for hydrogen peroxide and oxidase substrates. *Sensors and Actuators B: Chemical* **39**, 291–294 (1997).
6. YAMASHIRO, N. *et al*. Determination of Hydrogen Peroxide in Water by Chemiluminescence Detection, (I). *Journal of Nuclear Science and Technology* **41**, 890–897 (2004).
7. Brestovisky, A., KirowaEisner, E. & Osteryoung, J. Direct and titrimetric determination of hydrogen peroxide by reverse pulse polarography. *Anal. Chem.* **55**, 2063–2066 (2002).
8. Razmi, H. & Mohammad-Rezaei, R. Non-enzymatic hydrogen peroxide sensor using an electrode modified with iron pentacyanonitrosylferrate nanoparticles. *Microchim Acta* **171**, 257–265 (2010).
9. Bian, X. Z., Luo, H. Q. & Li, N. B. A New Material Based on Nanostructured Prussian Blue Analogue Film Doped with Ce(III) for Development of Hydrogen Peroxide Sensor. *Electroanalysis* **22**, 1364–1368 (2010).
10. Nia, P. M., Meng, W. P. & Alias, Y. Hydrogen peroxide sensor. Uniformly decorated silver nanoparticles on polypyrrole for wide detection range. *Applied Surface Science* **357**, 1565–1572 (2015).
11. Fan, J. *et al*. Formation of three-dimensional nano-porous silver films and application toward electrochemical detection of hydrogen peroxide. *Applied Surface Science* **285**, 185–189 (2013).
12. Zhang, N., Sheng, Q., Zhou, Y., Dong, S. & Zheng, J. Synthesis of FeOOH@PDA-Ag nanocomposites and their application for electrochemical sensing of hydrogen peroxide. *Journal of Electroanalytical Chemistry* **781**, 315–321 (2016).
13. Zhao, W. *et al*. A novel nonenzymatic hydrogen peroxide sensor based on multi-wall carbon nanotube/silver nanoparticle nanohybrids modified gold electrode. *Talanta* **80**, 1029–1033 (2009).
14. El-Nagar, G. A., Derr, I., Fetyan, A. & Roth, C. One-pot synthesis of a high performance chitosan-nickel oxyhydroxide nanocomposite for glucose fuel cell and electro-sensing applications. *Applied Catalysis B: Environmental* **204**, 185–199 (2017).
15. Bansal, V., Li, V., O'Mullane, A. P. & Bhargava, S. K. Shape dependent electrocatalytic behaviour of silver nanoparticles. *CrystEngComm* **12**, 4280 (2010).
16. Tian, J. *et al*. Preparation of Ag nanoparticle-decorated poly(m-phenylenediamine) microparticles and their application for hydrogen peroxide detection. *The Analyst* **136**, 1806–1809 (2011).
17. Maduraiveeran, G. & Ramaraj, R. Gold nanoparticles embedded in silica sol–gel matrix as an amperometric sensor for hydrogen peroxide. *Journal of Electroanalytical Chemistry* **608**, 52–58 (2007).
18. Guo, S., Wen, D., Zhai, Y., Dong, S. & Wang, E. Platinum nanoparticle ensemble-on-graphene hybrid nanosheet: one-pot, rapid synthesis, and used as new electrode material for electrochemical sensing. *ACS nano* **4**, 3959–3968 (2010).
19. Wang, J. *et al*. Detection of hydrogen peroxide at a palladium nanoparticle-bilayer graphene hybrid-modified electrode. *Sensors and Actuators B: Chemical* **230**, 690–696 (2016).
20. Šljukić, B. & Compton, R. G. Manganese Dioxide Graphite Composite Electrodes Formed via a Low Temperature Method. Detection of Hydrogen Peroxide, Ascorbic Acid and Nitrite. *Electroanalysis* **19**, 1275–1280 (2007).
21. Hrbac, J., Halouzka, V., Zboril, R., Papadopoulos, K. & Triantis, T. Carbon Electrodes Modified by Nanoscopic Iron(III) Oxides to Assemble Chemical Sensors for the Hydrogen Peroxide Amperometric Detection. *Electroanalysis* **19**, 1850–1854 (2007).
22. Wang, J., Xu, M., Zhao, R. & Chen, G. A highly sensitive H2O2 sensor based on zinc oxide nanorod arrays film sensing interface. *The Analyst* **135**, 1992–1996 (2010).
23. Bastús, N. G., Merkoçi, F., Piella, J. & Puntes, V. Synthesis of Highly Monodisperse Citrate-Stabilized Silver Nanoparticles of up to 200 nm. Kinetic Control and Catalytic Properties. *Chem. Mater.* **26**, 2836–2846 (2014).

24. Fuku, K. *et al.* The synthesis of size- and color-controlled silver nanoparticles by using microwave heating and their enhanced catalytic activity by localized surface plasmon resonance. *Angewandte Chemie (International ed. in English)* **52**, 7446–7450 (2013).
25. Zhang, B. *et al.* Acid-directed synthesis of SERS-active hierarchical assemblies of silver nanostructures. *J. Mater. Chem.* **21**, 2495–2501 (2011).
26. Muench, F. *et al.* Electrodeposition and electroless plating of hierarchical metal superstructures composed of 1D nano- and microscale building blocks. *Electrochimica Acta* **202**, 47–54 (2016).
27. Zhang, M. & Wang, Z. Nanostructured silver nanowires-graphene hybrids for enhanced electrochemical detection of hydrogen peroxide. *Appl. Phys. Lett.* **102**, 213104 (2013).
28. Kurowska-Tabor, E., Jaskuła, M. & Sulka, G. D. Sensitive Amperometric Sensing of Hydrogen Peroxide Using Ag Nanowire Array Electrode. *Electroanalysis* **27**, 1968–1978 (2015).
29. Meng, Z., Zhang, M., Zhang, H. & Zheng, J. A sensitive hydrogen peroxide sensor based on leaf-like silver. *Meas. Sci. Technol.* **25**, 25301 (2014).
30. Han, Y., Zheng, J. & Dong, S. A novel nonenzymatic hydrogen peroxide sensor based on Ag–MnO2–MWCNTs nanocomposites. *Electrochimica Acta* **90**, 35–43 (2013).
31. Li, Y., Lu, Q., Wu, S., Wang, L. & Shi, X. Hydrogen peroxide sensing using ultrathin platinum-coated gold nanoparticles with core@shell structure. *Biosensors & bioelectronics* **41**, 576–581 (2013).
32. Zhang, Y. *et al.* Nano-assemblies consisting of Pd/Pt nanodendrites and poly (diallyldimethylammonium chloride)-coated reduced graphene oxide on glassy carbon electrode for hydrogen peroxide sensors. *Materials science & engineering. C, Materials for biological applications* **58**, 1246–1254 (2016).
33. Ye, Y. *et al.* Enhanced nonenzymatic hydrogen peroxide sensing with reduced graphene oxide/ferroferric oxide nanocomposites. *Talanta* **89**, 417–421 (2012).

Acknowledgements

Author Contributions

Gumaa A. El-Nagar: Create the idea and measured the electrochemical tests and characterized the as-prepared microstructures using XRD and XPS. In addition, wrote the manuscript and prepared the figures and replies to the reviewer´s comments. Radwan M. Sarhan: Prepared the silver microstructures and contributed in writing of the first manuscript draft. Ahed Abouserie: Imaged the as-prepared catalysts by SEM. Matias Bargheer: Revised the manuscript and help in improved the manuscript quality. Natalia Maticiuc & Iver Lauermann: XPS measurements Christina Roth: Reviewed the manuscript, modified/improved the figures representation and shared the idea. Besides, her valuable comments/discussions improved the quality of the manuscript.

Additional Information

Competing Interests: The authors declare that they have no competing interests.

Publisher's note: Springer Nature remains neutral with regard to jurisdictional claims in published maps and institutional affiliations.